Finite-size criticality in fully connected spin models on superconducting quantum hardware

Michele Grossi,[1,*] Oriel Kiss,[1,2] Francesco De Luca,[3] Carlo Zollo,[3] Ian Gremese,[3] and Antonio Mandarino[4,†]

[1] *European Organization for Nuclear Research (CERN), Geneva 1211, Switzerland*
[2] *Department of Particle and Nuclear Physics, University of Geneva, 1211 Geneva, Switzerland*
[3] *Department of Physics, University of Trieste, 34127 Trieste, Italy*
[4] *International Centre for Theory of Quantum Technologies, University of Gdańsk, Wita Stwosza 63, 80-308 Gdańsk, Poland*

The emergence of a collective behavior in a many-body system is responsible of the quantum criticality separating different phases of matter. Interacting spin systems in a magnetic field offer a tantalizing opportunity to test different approaches to study quantum phase transitions. In this work, we exploit the new resources offered by quantum algorithms to detect the quantum critical behaviour of fully connected spin$-1/2$ models. We define a suitable Hamiltonian depending on an internal anisotropy parameter γ, that allows us to examine three paradigmatic examples of spin models, whose lattice is a fully connected graph. We propose a method based on variational algorithms run on superconducting transmon qubits to detect the critical behavior for systems of finite size. We evaluate the energy gap between the first excited state and the ground state, the magnetization along the easy-axis of the system, and the spin-spin correlations. We finally report a discussion about the feasibility of scaling such approach on a real quantum device for a system having a dimension such that classical simulations start requiring significant resources.

I. INTRODUCTION

The abrupt change of the system properties during a phase transition has always paved the way to the advancement of our understanding of nature in both fundamental and applied aspects. The phase transition mechanism, in the limit of an infinite number of particle composing the system, has been successfully addressed within the formalism of the renormalization group [1, 2]. Quantum phase transitions are the cornerstone of a great variety of groundbreaking theories ranging from the Higgs mechanism for mass generation in high-energy physics [3, 4], to the superfluid and superconducting phase of matters in low-energy physics [5, 6], and nowadays their exploitation is getting attention also in the context of quantum technologies [7, 8].

Given a Hamiltonian $H(\vec{\lambda})$, describing a system constituted by N interacting particle, it exhibits a continuous (or second order) quantum phase transition, whether in the limit $N \to \infty$, the gap between the ground state energy and that of the first excited state vanishes for a certain value of the internal parameters $\vec{\lambda}$. This value corresponds to the critical point of the model and, in contrast to any classical model, it can also exist for zero temperature [9, 10]. Nevertheless, assuming a diverging number of particle is well motivated and substantiated. The relaxation of such assumption prompts the study of finite-size corrections to such transition [11, 12] that can show unprecedented results [13–15]. With abuse of notation we write that a quantum phase transition occurs in a system with finite N, whenever for a value of $\vec{\lambda}$, a crossing between the energies of the ground state and the first excited level is observed. This is in contrast to what one would expect by a semi-classical approach in which the finite size is responsible to suppress the symmetry breaking mechanism associated with the second-order phase transition [11, 16].

For our purposes, we consider the Lipkin-Meshkov-Glick (LMG) model, a fermionic model that served as testbed for many-body approximations in different fields [17–19]. Due to the possibility of mapping this model into a N spin$-1/2$ system, we will study its criticality with current quantum computation techniques on real Noisy-Intermediate-Scale Quantum (NISQ) devices. Criticality of quantum system requires an exponential number of degrees of freedom that makes the problem quickly intractable. The advancement of machine learning techniques has been of paramount importance for the determination of macroscopic phases of matter and efficient quantum state representation.

With the advent of quantum techniques in machine learning, phase diagram of different systems have been obtained, such as a cluster Ising or the Bose-Hubbard model at zero temperature. The former uses a supervised learning approach where the states are classified according to classical labels using a quantum convolutional neural network [20, 21] while the latter discovers the phases in an unsupervised way using anomaly detection [22]. The intersection between machine learning and quantum techniques applied to physical systems is rapidly increasing, not only obtaining information about critical point of a system is pursued but also general dynamical simulations are important testbeds. In [23] the authors rigorously analyze the requirements of an algorithm in terms of training data and define generalization bounds for their effective execution on current quantum device. For an overview of the state of the art and future

* michele.grossi@cern.ch
† antonio.mandarino@ug.edu.pl

perspectives for quantum simulation, looking at possible quantum advantage in specific applications we refer to [24].

The remainder of this manuscript is structured as follows: in Sec.II we introduce the LMG Hamiltonian of our critical system, then we provide a short but comprehensive introduction to the variational quantum eigensolver technique. Then we focus on the definition of the ansatz in terms of design and trainability and we terminate the section providing an overview of the adopted error mitigation techniques, with ad-hoc consideration for the specific Hamiltonian. In Sec III, we substantiate our approach showing simulated results obtained under ideal condition with quantum simulator as well as evidences collected on real quantum device. In Sec. IV, we provide a numerical interpretation and analytical derivation of higher order excited states for the LMG model, as well as their realisation with the variational algorithm. Finally in Sec. V, we summarise the outcomes of this work, discussing the quality of the results with an estimation about the actual feasibility of studying proposed models-like on NISQ devices.

II. METHODS

In this section we introduce the Hamiltonian of a LMG critical system and its behaviour in the thermodynamic limit. Moreover, we review also the quantum computational techniques that we employ to assess the critical behavior of the system.

A. The Lipkin-Meshkov-Glick Model

The LMG model was introduced in [17–19] to describe a system of N fermions, whose state space is made of two degenerate shells with two fixed energy levels. Each shell has degeneracy N and can accommodate all of the N particles, thus resulting in a total of a 2^N-dimensional state space. Via a Jordan-Wigner transformation, the LMG model can be mapped into a system of interacting spins. Moreover, in the thermodynamic limit $N \to \infty$, it is solvable via a two-boson Holstein Primakoff transformation [25]. This peculiarity made it one of the most used model to understand many problems of interest in physics, from nuclear to condensed-matter physics.

Considering that we will study our model on qubit-based quantum computers, it is natural and convenient to use the following expression for the LMG Hamiltonian:

$$H = -\frac{1}{N}\sum_{i<j}^{N} \sigma_x^i \sigma_x^j + \gamma \sigma_y^i \sigma_y^j - B\sum_{i=1}^{N} \sigma_z^i. \qquad (1)$$

This Hamiltonian describes a system of N spins in a fully connected planar graph, immersed in a transverse magnetic field B. The first sum in Eq.(1) accounts for an anisotropic interaction in the $x-y$ plane that couples each spin with all the other ones with the same strength, an archetype and exemplary version of any long-range interaction. Different coupling strengths along the two planar direction are taken into account via the anisotropy parameter $0 \leq \gamma \leq 1$. From physical perspective, this type of Hamiltonian has been implemented on various platforms [26–29] to design feasible quantum technologies applications [30–34].

The system is known to be critical and shows, in the thermodynamic limit, a second order phase transition between a broken-symmetry (disordered) phase for $B < 1$ and an ordered phase for $B \geq 1$, with a critical value of the external magnetic field $B = B_c = 1$. Usually, the Lipkin model is used to denote a limiting and easily diagonalizable case of the LMG model [35]. Introducing the set of collective-spin operators $S_\alpha = \frac{1}{2}\sum_{i=1}^{N} \sigma_\alpha^i$, and setting $\gamma = 1$ in Eq.(1), we have:

$$H = -\frac{2}{N}(\mathbf{S}^2 - S_z^2) - 2BS_z. \qquad (2)$$

The Hamiltonian in Eq.(2) is diagonal in the Dicke basis $|j,m\rangle$ formed by the simultaneous eigenvectors of $\mathbf{S}^2 |j,m\rangle = j(j+1)|j,m\rangle$ and $S_z |j,m\rangle = m|j,m\rangle$. Due to the fact that the interaction term commutes with the free energy term, the Lipkin model with $\gamma = 1$ belongs to a different universality class of the general model described by the Hamiltonian in Eq.(2), see [25]. In particular, it has been shown to belong to the same class of the superradiant Dicke model [36]. Within our formalism, we can also address the criticality of the fully-connected Ising model imposing $\gamma = 0$. This model presents, in the thermodynamical limit, a quantum phase transition due the spontaneous breaking of the $\mathbb{Z}_2$ symmetry [37].

The phase diagram of this model at zero temperature was derived in [38], thanks to a two-boson Schwinger boson realization of the $SU(1,1)$ Richardson–Gaudin integrable models. However, classifying phase transitions in systems having finite number of elements is a challenging and an open problem. In particular, in the quantum domain, the curse of dimensionality of the exponentially growing size of the Hilbert space for the considered systems impacts strongly the performance of classical techniques.

We will study the precursors of the quantum phase transition for the finite size LMG model via quantum computational techniques. With abuse of notation, we will call the values of the magnetic field B and of the anisotropy γ, for which the ground state and the first excited state of the system are degenerate, critical values.

The adopted strategy can be easily extended to other critical systems, but the choice of the LMG model to test our approach is driven by two reasons. On one side, the model is of interest for several communities and it has been used to test many-body approximations [25, 39]. The expression in Eq.(1), in terms of Pauli operators, makes the implementation on a superconducting quantum processor quite straightforward and requires less

physical resources compared with its fermionic formulation. On the other side, the model has some peculiarities, namely anisotropy and long-range interaction, that makes it a non trivial model where to assess quantum criticality at finite-size.

B. Variational Quantum Eigensolver

The Variational Quantum Eigensolver (VQE), proposed by Peruzzo *et al.* [40], is a variational quantum algorithm [41] used to find the ground state of a Hamiltonian H by using the Rayleigh-Ritz variational principle. Concretely, a parametrized wavefunction $|\psi(\theta)\rangle$ [42] is prepared on a quantum computer and its parameters updated to minimize the energy

$$E_0 \leq \frac{\langle\psi(\theta)|\, H\, |\psi(\theta)\rangle}{\langle\psi(\theta)|\psi(\theta)\rangle}. \tag{3}$$

The VQE has been widely applied in quantum chemistry [43–46], nuclear physics [47–49] and in spin systems [50–56].

The design of the wavefunction ansatz is of importance for the trainability and accuracy of the results and is an active area of research. Some systems, typically written in the second quantisation formalism, allow physically motivated ansätze, for instance based on unitary coupled cluster [43, 48]. However, the quantum circuits used in this setting are usually deep, require an increased connectivity, and are therefore difficult to implement on near term quantum devices. On the other hand, hardware efficient ansatz [44] are tailored to the device and are consequently shallow enough to minimize the effects of noise and decoherence. More recently, the ADAPT-VQE [57], which builds the ansatz by iteratively adding a term from an operator pool bringing the best improvement, has been proposed as a way to build optimal circuits. Even if the picking action can be implemented in a parallel fashion, it can be expensive for current devices, time and resources-wise. Consequently, we will focus on fixed hardware efficient ansätze, which are constructed with single qubit rotations around the y-axis, and CNOT interactions with linear connectivity.

The VQE can be extended to compute excited states as well. The method adopted here is the one proposed by Higgott *et al.* [58], called *variational quantum deflation* (VQD), which first computes the ground state and then looks for the state minimizing the energy while being orthogonal to the, previously determined, ground state. This procedure can be generalize for the k-th excited state in an iterative fashion. In practice, the following loss function is minimized:

$$F(\theta_k) = \langle\psi(\theta_k)|\, H\, |\psi(\theta_k)\rangle + \sum_{i=0}^{k-1} \beta_i \langle\psi(\theta_k)|\psi(\theta_i)\rangle\,, \tag{4}$$

where we assume, for simplicity, that the states are normalized. The wavefunction $|\psi(\theta_i)\rangle$ corresponds to the i-th excited state, and β_i hyperparameters to be tuned. It has been shown [58], that β_i has to be greater than the energy gap between the states i and $i+1$ to ensure that the wavefunction converges to the correct excited state. Additional techniques, based on the quantum equation of motion [59], using a discriminator [60] or constraining the ansatz around the state of interest [61] have been proposed in the literature but will not be considered here.

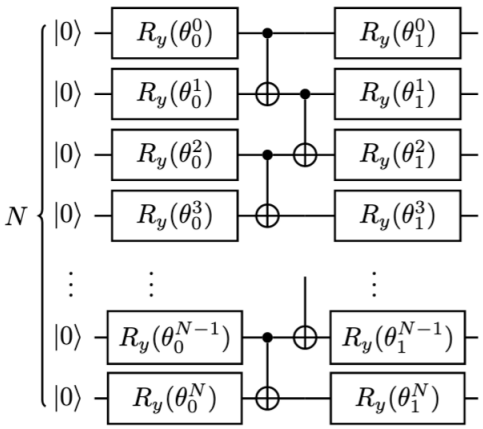

Figure 1. Hardware efficient ansatz, composed of $R_y(\theta)$ rotations and CNOTs between neighboring qubits executed in parallel.

C. Ansatz

We use a simple hardware efficient ansatz [44], which can be run on NISQ devices without an overhead due to circuit transpilation. For instance, we use D repetitions of a layer consisting of free rotations around the y-axis $R_y(\theta) = e^{-i\theta\sigma_y/2}$, where σ_y is the y Pauli matrix, CNOT gates with linear connectivity and a final rotation layer before the measurements. Since the depth of the circuits grows as $\mathcal{O}(N)$ due to the linear entanglement, this ansatz fails on hardware when performing error mitigation based on noise scaling. We therefore adapt the ansatz to grow as $\mathcal{O}(1)$, by applying the CNOT gates in parallel, on the two following groups of qubits

$$\{(i, i+1) \text{ for } i \text{ even}\},$$
$$\{(i, i+1) \text{ for } i \text{ odd}\},$$

thus considerably reducing the depth of the circuits. We observe a small decrease in the accuracy on the simulator compared to the linear entanglement scheme, but an increase on the hardware due to the depth's reduction. We choose the minimal case $D = 1$, as depicted in Figure 1, when running on hardware, while pushing for maximal performance on the simulator by allowing larger D.

D. Error Mitigation

Error mitigation methods are used to diminish the effect of the hardware noise on the results. Unlike error correction, these strategies are used in the post-processing steps on the raw data. Two complementary techniques, measurement error mitigation (MEM) and zero noise extrapolation (ZNE), are used to mitigate the readout and two-qubit gate errors, respectively.

For MEM, we follow Nation *et al.* [62] and individually invert the error matrices

$$M^k = \begin{pmatrix} P_{0,0}^{(k)} & P_{0,1}^{(k)} \\ P_{1,0}^{(k)} & P_{1,1}^{(k)} \end{pmatrix} \tag{5}$$

and used them to calibrate the samples. Here, $P_{i,j}^{(k)}$ is the probability of the k-th qubit to be in state $j \in \{0,1\}$ while measured in state $i \in \{0,1\}$. The probabilities of measuring 0 or 1

$$\vec{S}^k = \begin{pmatrix} P_0 \\ P_1 \end{pmatrix} \tag{6}$$

obtained by measuring the k-th qubit are corrected as follow

$$\vec{S}^k_{\text{corrected}} = (M^k)^{-1}\vec{S}^k. \tag{7}$$

While this only corrects uncorrelated readout errors, it is argued in Ref. [62] that they are the predominant ones. Moreover, this strategy can be scaled for arbitrary number of qubits and only has a $\mathcal{O}(1)$ overhead in the number of circuit execution.

In the ZNE [63, 64] scheme, the CNOT noise is artificially stretched and the results are then extrapolated to the noiseless regime. More precisely, the energy is estimated multiples time for different scaling factor $k \in \{1,2\}$, and then a fit is performed to extrapolate up to the $k = 0$ value. In practice, the noise is stretched by replacing every CNOT in the circuit, by $2k-1$ CNOT gates. The $2k-2$ additional CNOTs cancel each other, leaving the circuit unchanged. However, by adding barriers between them, preventing the CNOTs to be cancelled in the transpilation phase, the noise is artificially stretched. Richardson [65] originally used a linear fit for the extrapolation, however, the considerable effect of the noise in NISQ devices increases the risk of overshooting. Consequently, an exponential fit $f(x) = ae^{bx}$ is instead used, where a and $b \in \mathbb{R}$ are fitted to the energies E using least-square regression. To improve the results, E is scaled before the fit

$$E \mapsto \frac{E-s}{s} \tag{8}$$

and scaled back afterwards, with s being an estimate of the exact energy.

It is important to make sure that the total runtime of the noise-scaled circuits does not exceed the coherence time of the device, which would destroy any useful information. For instance, we only considered $k = 1$ and $k = 2$, since for higher k the results were not reliable anymore. Also the ansatz definition plays an important role, as described in sec.II C. With the construction of Figure 1, the CNOT gates can be run in parallel, thus shortening the runtime significantly. This can be done using additional qubits available on the device to run all the noise-scaled circuits in parallel, reducing the total number of circuit execution.

III. RESULTS

This section presents the numerical results obtained in this work. Sec. III A contains the ground and first excited state energy and magnetization for $N = 4, 5, 6$ spins and different values of γ and B obtained on statevector simulations and analyse their behaviour in the anisotropic and isotropic case. Sec. III B shows the ground state energy and magnetization for $N = 5$ spins, $\gamma = 0.49$ and different values of B computed on superconducting transmon qubits, and comments on the scalability of the VQE in the near term.

A. Noiseless VQE Simulations

For a small number of spins N, the classical approach of the diagonalization of H is straightforward. Defining the spectrum of the Hamiltonian $H|\psi_n\rangle = E_0|\psi_n\rangle$ with $n = \{0, ..., 2^{N-1}\}$, multiple crossing points between the energies of the ground and the first excited state (E_0 and E_1, respectively) are found for the following critical values

$$B_C^k = \frac{N-k}{N}\sqrt{\gamma}, \tag{9}$$

for a fixed γ, $k \leq N$ and odd [39]. Hence, the ground state energy can be recasted in $N/2+1$ *phases*, if N is even, or in $(N-1)/2+1$ otherwise. Introducing the ground-state magnetization along the model easy-axis $\langle S_z\rangle = \langle\psi_0(B,\gamma)|S_z|\psi_0(B,\gamma)\rangle$, we can observe that for any nonanalytic point holds $\lim_{B\to B_C^{k-}}\langle S_z\rangle \neq \lim_{B\to B_C^{k+}}\langle S_z\rangle \,\forall\, B_C^{(k)}$. In the following, we will denote $|\psi_0\rangle \equiv |\psi_{GS}\rangle$ and $|\psi_1\rangle \equiv |\psi_{1st}\rangle$.

We use statevector simulations, as a theoretical tool to explore more complex ansatz and increase the performance as much as possible. We choose the depth of the ansatz as a function of the system size, namely $D = N$. This differs from the results obtained on real hardware, as explained in Sec. II C. The training is performed with the SLSQP optimizer [66] with 2000 maximum iterations. Adiabatic computing is applied to speed up the calculations and improve the accuracy, following the recommendation of Harwood *et al.* [67]. The excited states are found using a VQD-like algorithm. Using the statevector

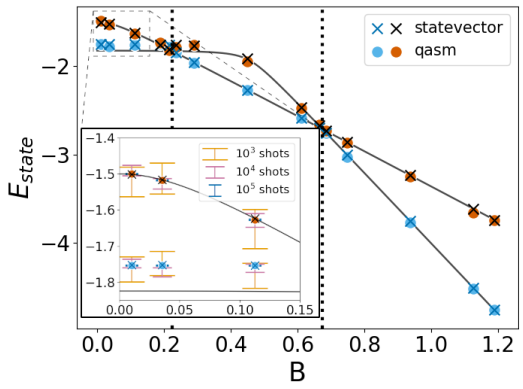

Figure 2. Ground and first excited state energies for 4 spins at $\gamma = 0.81$ obtained with classical diagonalization and VQE using statevector and QASM without noise. VQE results are represented by crosses, exact diagonalization by a solid line, while dotted lines show crossing points. The inset shows result obtained with different number of shots, where the error bar correspond to one standard deviation.

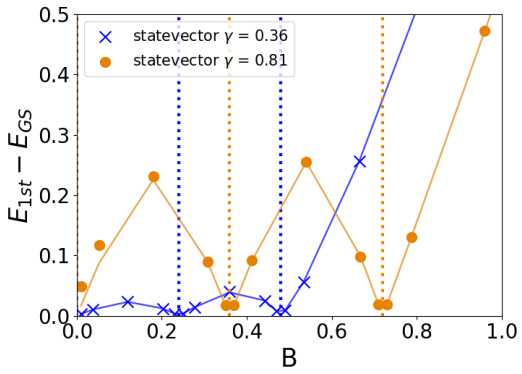

Figure 3. First excited state and ground state energy difference for $N = 5$ at $\gamma = 0.36, 0.81$. VQE results are represented by crosses, exact diagonalization by a solid line, while dotted lines show crossing points.

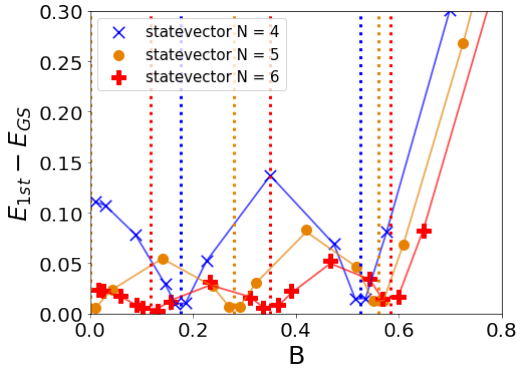

Figure 4. First excited state and ground state energy difference at $\gamma = 0.49$ for $N = 4, 5, 6$. VQE results are represented by crosses, exact diagonalization by a solid line, while dotted lines show crossing points.

given by the solution of the Hamiltonian it is possible to redefine a new effective Hamiltonian

$$H' = H + \beta_0 \left|\psi_{GS}\right\rangle \left\langle\psi_{GS}\right| . \tag{10}$$

When the superposition between $|\psi_{1st}\rangle$ found by using VQE on H' and $|\psi_{GS}\rangle$ is small the loss function associated to this Hamiltonian reduces to Eq.(4) with $k = 1$. We found this to be true every time the β_0 is set greater than the energy gap between the ground and first excited state, as specified in Sec.II B. Knowing that transitions happen for $B = B_C^k$, see Eq.(9), we choose five points between the transition points and the chosen bounds. Starting from the upper bound, where the energy gap is wider, the ground state energy and the first excited energy are evaluated using random initial parameters. For each point in the interval, in decreasing order, the optimal point found in the previous step are chosen as initial parameters. Moreover, for the next interval, the optimal parameters for the ground state are used as initial point as well for the first excited state. This technique significantly speeds up the simulation, improves the quality of the results, and allows us to compute the energies for systems up to $N = 10$ spins, using statevector simulations.

Figure 2 shows the ground and first excited state energy for a LMG Hamiltonian with $N = 4$ spins for the specific value of $\gamma = 0.81$, as a function of the magnetic field B. The VQE is compared to the exact diagonalization (black solid lines), while the VQE points are obtained using statevector simulation (crosses) as well as shoots-based probabilistic output without hardware noise contribution (dots). Another figure of merit to assess a quantum phase transition for finite-size systems is the energy difference between the first excited state and the ground state, namely $E_{1st} - E_{GS}$ (to which we will refer to as the gap, for shorthand of notation). The gap as a function of the magnetic field is shown in Figure 3 for $N = 5$ spins and two values of γ, $\gamma = 0.36, 0.81$. Even if they are far from the extreme values $0, 1$ they already underline a difference in the behaviour, at least for $B < 0.6$. Similar considerations hold as a function of the system size, shown in Figure 4 for $N = 4, 5, 6$ with $\gamma = 0.49$. In both cases, the energy gap rapidly explodes after $B \geq 0.6$. Finally, we consider the extreme cases of the fully-connected Ising model and the Lipkin-Dicke model, for $\gamma = \{0, 1\}$ respectively. We report our results in Figure 5, together with an intermediate γ value of 0.49, where the system size is fixed to $N = 5$. The energy gap between the first excited state and the ground state is shown in (a), while the correlation function along x $\left\langle S_x^2 \right\rangle$ in (b) and $\langle S_z \rangle$ in (c). We observe the oscillatory trend of the energy gap for $\gamma = 1$ as opposed to the monotonic trend of the isotropic case ($\gamma = 0$). A completely different behaviour can be appreciated also for the two magnetization observable, where the anisotropic model is characterised by a stepwise trend as opposed to the continuous one for $\gamma = 0$, signaling how the three models in the thermodynamical limit belong to distinct universality classes.

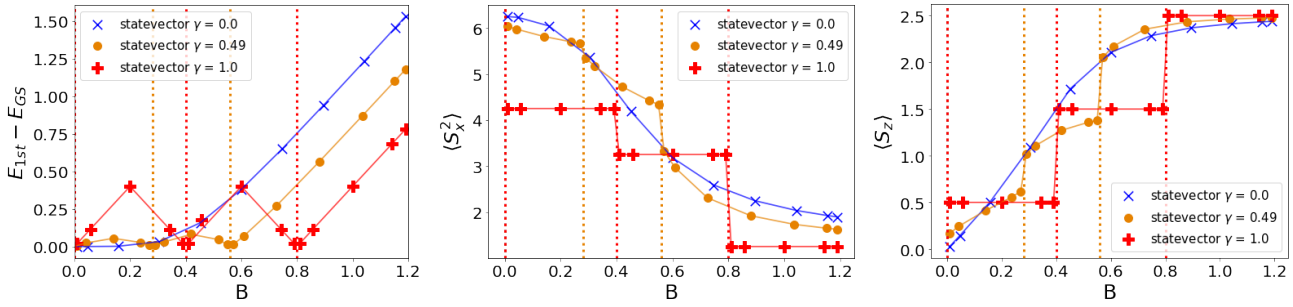

Figure 5. Ground state energy (GS) and first excited state energy (1st) gap (a), $\langle S_x^2 \rangle$ (b), and $\langle S_z \rangle$ (c), for $N = 5$ spins at $\gamma = 0, 0.49, 1$ values. VQE results are represented by crosses, exact diagonalization by a solid line, while dotted lines show crossing points.

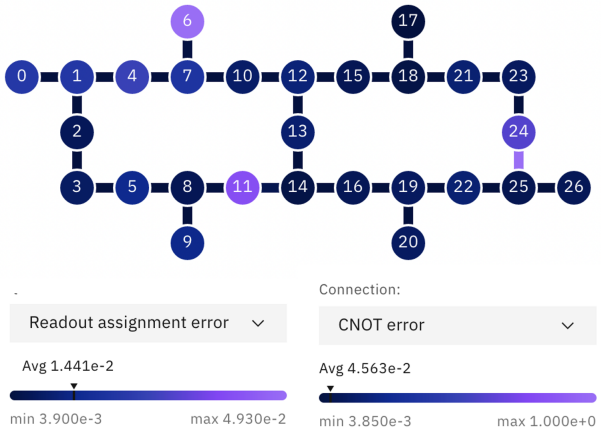

Figure 6. Topology of the superconducting quantum device ibmq_kolkata with readout and CNOT error rate. Image taken from the IBM Q Lab.

B. Runs on the Real Devices.

1. Experimental Device

The quantum device used in this work consists of 27 fixed-frequency transmons qubits, with fundamental transition frequencies of approximately 5 GHz and anharmonicities of −340 MHz, with the same topology as displayed in Figure 6. Microwave pulses are used for single-qubit gates and cross-resonance interaction [68] for two-qubit gates. The experiments took place over 1 month, but each different computation took place over span of five hours, without intermediate calibration, with the use of Qiskit Runtime. The median qubit lifetime T_1 of the qubits is 121 and 129 μs, the median coherence time T_2 is 90 and 135 μs and the median readout and CNOT error is 0.014 and 0.045 respectively. The SABRE [69] algorithm is used for the transpilation to the quantum hardware.

2. Small System Size

We begin by computing the ground state energy of a system with $N = 5$ spins and $\gamma = 0.49$ for different values of the magnetic field B. We use the hardware efficient ansatz with $D = 1$ repetition, as shown in Figure 1. As a warm initialization, the ansatz is first trained on the noiseless simulator, and the optimal parameters are used as an educated guess for the initial parameters. The training is composed of maximum 100 steps, or until convergence, with the SPSA [70] optimizer using a learning rate of 0.005 for the first 30 steps and 0.001 afterwards, using 8092 shots. The graphs are obtained with 32000 shots and statistics are collected from 5 distinct runs. Measurement error mitigation and zero noise extrapolation are performed to enhance the results, which are shown in Figure 7. The line correspond to the exact diagonalization, the black dots to the noiseless simulation with 32000 shots, the blue crosses to the raw results and the red ones to the mitigated energies. The error bars correspond to the 99.5 % confidence interval. The inset shows the effect of the error mitigation on a specific point. The $k = 1$ point correspond to the original circuit while $k = 2$ to the dilated case, where every CNOT is replaced with 3 CNOTs. The cross shows a scaled exponential fit while the triangle a linear one. As motivated in Sec. II D, the linear fit overshoots the true ground state energy, while this is not the case for the scaled exponential fit.

We observe that the ground state energy is reproduced with less than 1% error ratio everywhere, suggesting that the quality of current devices is good enough for such tasks. However, the computed magnetization observables are not equally accurate. The explanation is two folds: first, we observe that the noiseless simulations are also less precise than the energy calculations, more particularly for $\langle S_x^2 \rangle$ at large magnetic field. This is essentially caused by the ansatz which is too shallow to represent the true ground state, but instead is only a good approximation with similar energy. But more importantly, there is a discrepancy between the noiseless and real hardware results, which is due to overfitting to the hardware noise.

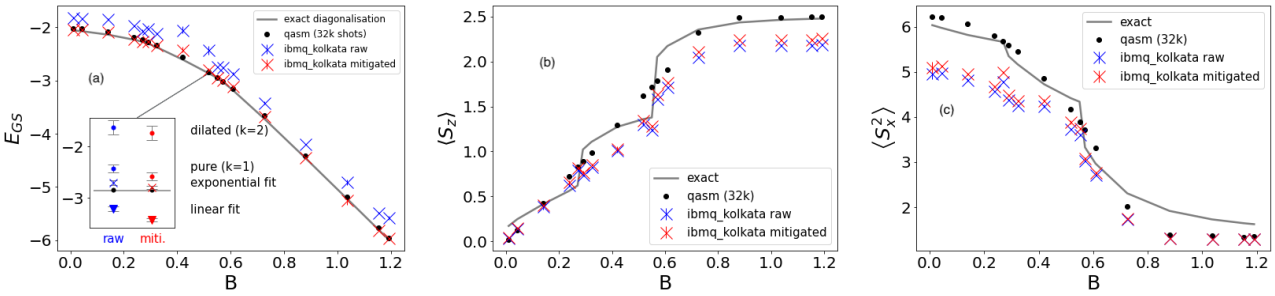

Figure 7. Ground state energy (GS) (a), and magnetization $\langle S_x^2 \rangle$ (b), and $\langle S_z \rangle$ (c), for $N = 5$ spins at $\gamma = 0.49$ values. Points are obtained on the superconducting device ibmq_kolkata with (red) and without (blue) error mitigation compared to noiseless simulation (black) and exact values (line). The inset shows the extrapolation to the zero noise regime, both with an exponential and linear fit.

Hence, when the ansatz is fine tuned on the real device, the noise is assimilated to minimze the energy. By doing so, we get closer to the true energy, but drift from the true ground state. Hence, the ansatz is good to reproduce the energy, but does not represent the true ground state.

3. *Large System Size*

Finally, we tried to extend the reach of VQE to sizes where simulations are unavailable due to the exponential scaling of the Hilbert space. Even if density-matrix renormalization group (DMRG) [71] techniques are able to compute the ground state energy for large number of spins ($\sim 10^2$), we choose $N = 20$ since it is already out of reach for our simulators in a reasonable time. This problem is more interesting than the previous case since we are unable to start from a set of previously trained parameters. However, these calculations are also more challenging for current devices for the following reasons. Gradient-free optimizers, such as SPSA, require small amount of circuit executions to estimate the gradient. However, since they rely on finite difference techniques, the gradient is strongly affected by the noise and can lead to erratic path in the optimization landscape. On the other hand, analytical gradients provided by the parameter-shift rule [72] are more reliable, but also more expensive to compute since they require $2 \cdot d$ circuit executions, where d is the number of parameters ($d = 40$ in this case). We estimate to more than one hour runtime per optimizer step, accounting for ZNE and MEM error mitigation techniques, which is more than what we can reasonably draw from on a shared device and without running into further recalibration problems.

IV. HIGHER EXCITED STATES

The VQE can be used to compute the energies of the second and third excited states as well. Figures 8 and 9 show the eight lowest energy eigenvalues for a system of $N = 4$ spins, as a function of the magnetic field B at two different interaction configurations $\gamma = \{1, 0.67\}$, respectively. The simulations are performed using statevector and superimposed to exact diagonalization. For $\gamma = 0.67$, VQE seems at first to fail in computing the

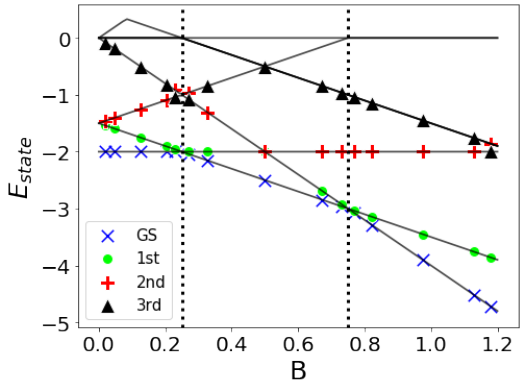

Figure 8. Excited states energy for $N = 4$ and $\gamma = 1$. Solid lines are for classical results, dotted lines for crossing points.

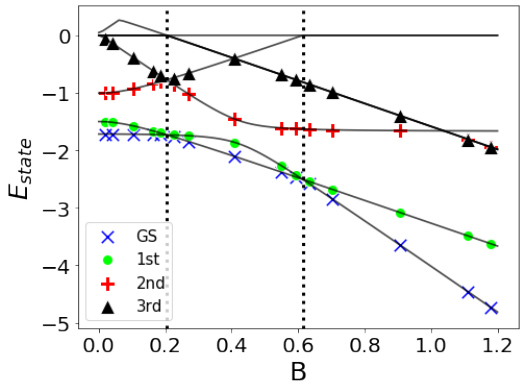

Figure 9. Excited states energy distribution for $N = 4$ and $\gamma = 0.67$. Solid lines are for classical results, dotted lines for crossing points.

3rd excited state, but actually find degenerate states. To better understand the degeneracy, let us consider $\gamma = 1$ and use Eq. 2 to obtain

$$H\,|j,m\rangle = \left[-\frac{1}{2}(j(j+1) - m^2 - 2) - 2Bm\right]|j,m\rangle\,. \quad (11)$$

For $N = 4$ spins, $j = 0, 1, 2$, leading to 9 distinct degenerate values for the energies of the 16 eigenstates. The first degenerate eigenvalue for $B < \frac{1}{4}$, is the one with the $j = 1$, $m = 1$ quantum numbers. However, it becomes the fourth excited for $\frac{1}{4} < B < \frac{1}{2}$, the third for $\frac{1}{2} < B < \frac{5}{4}$, and finally the second for B greater than $\frac{5}{4}$. Numerical investigations suggest an analogous behaviour for $\gamma \neq 1$ and $0 < \gamma \lesssim 2$. In the region $B \lesssim \frac{5}{4}\sqrt{\gamma}$, the first eigenvalue to be degenerate is the third excited while in $B \gtrsim \frac{5}{4}\sqrt{\gamma}$, it is the second excited. Hence, VQE actually shows in Figure 9 that for $B \approx 1.2$, the third eigenvalue is degenerate (3 times, in particular). The numerical investigations for $\gamma = 1$ show that the degenerate levels are

- 3-fold: $j = 1$, $m \in \{0, \pm 1\}$,
- 2-fold: $j = 0$, $m = 0$,

in agreement with [36]. A similar argument can be addressed also to justify the behaviour of the energies of the excited states for the model with $\gamma \neq 1$ as those observed in Figure 9. However, the impossibility to diagonalize the two terms of the Hamiltonian in a common basis would make the argument only less intuitive and more cumbersome.

V. DISCUSSION AND OUTLOOKS

The advent of reliable quantum hardware, although not yet fault-tolerant, has paved the way to novel techniques to tackle problems from different research areas. A natural avenue of research is the one that incorporates the quantum computing techniques to understand the physics of complex systems as many-body systems. To this end, we have proposed a way to exploit the variational quantum eigensolver, and the algorithms stemmed from it, for studying the finite-size criticality of paradigmatic spin models. Upon introducing a Hamiltonian with an anisotropic interaction γ in the $x - y$ plane we have studied the level crossings between the ground-state and the first-excited state in the proper LMG ($0 < \gamma < 1$) and in the two limit cases: the fully connected Ising model ($\gamma = 0$) and the Lipkin-Dicke model $\gamma = 1$. We used as figure of merit some relevant magnetic observables, i.e., the magnetization along the field direction and the spin-spin correlation along the $x-$axis.

Due to the geometry of the system, no lenght scale of the correlation can be defined, this makes the fully-connected spin models interesting systems to look for unconventional results at finite-size [25, 39] or to give a quantitative evaluation of the quality of a new computational or experimental technique [26, 30, 35]. Recently, several papers [52–55] addressed the Lipkin model on a quantum computer to question whether techniques and methods proper of quantum machine learning can be employed in nuclear physics. In general, the authors rely on system size of relatively small dimensions $N \leq 4$ performing a preliminary noiseless analysis for the isotropic model that can be analytically solved exactly.

Our analysis is complementary to those previously carried out and go into the direction of employing quantum algorithms to have a direct insight on problems of relevance in statistical physics. In fact, we have shown that the VQE is a powerful tool to assess the quantum phase transition of critical systems of finite-size. We have also addressed how to mitigate the errors present when employing NISQ devices and how it is feasible on a real hardware based on superconducting transmon qubits.

As final remark and open question we surmise that our method could be employed in future, when better performing hardware, with more qubits will be available, as a benchmark for the renormalization group approaches used to study the finite-size scaling behaviour of quantities of interest in statistical and condensed matter theory.

ACKNOWLEDGMENTS

AM is supported by Foundation for Polish Science (FNP), IRAP project ICTQT, contract no. 2018/MAB/5, co-financed by EU Smart Growth Operational Programme, and (Polish) National Science Center (NCN), MINIATURA DEC-2020/04/X/ST2/01794. MG and OK are supported by CERN Quantum Technology Initiative.

Access to the IBM Quantum Services was obtained through the IBM Quantum Hub at CERN. The views expressed are those of the authors and do not reflect the official policy or position of IBM or the IBM Q team.

[1] Jean Zinn-Justin, *Phase transitions and renormalization group* (Oxford University Press on Demand, 2007).
[2] Andrea Pelissetto and Ettore Vicari, "Critical phenomena and renormalization-group theory," Physics Reports **368**, 549–727 (2002).
[3] F. Englert and R. Brout, "Broken symmetry and the mass of gauge vector mesons," Phys. Rev. Lett. **13**, 321–323 (1964).
[4] Peter W. Higgs, "Broken symmetries and the masses of gauge bosons," Phys. Rev. Lett. **13**, 508–509 (1964).
[5] J. Bardeen, L. N. Cooper, and J. R. Schrieffer, "Theory of superconductivity," Phys. Rev. **108**, 1175–1204 (1957).

[6] David R Tilley and John Tilley, *Superfluidity and superconductivity* (Routledge, 2019).

[7] Luigi Amico, Rosario Fazio, Andreas Osterloh, and Vlatko Vedral, "Entanglement in many-body systems," Rev. Mod. Phys. **80**, 517–576 (2008).

[8] Florian Schäfer, Takeshi Fukuhara, Seiji Sugawa, Yosuke Takasu, and Yoshiro Takahashi, "Tools for quantum simulation with ultracold atoms in optical lattices," Nature Reviews Physics **2**, 411–425 (2020).

[9] Subir Sachdev, *Quantum Phase Transitions*, 2nd ed. (Cambridge University Press, 2011).

[10] S. L. Sondhi, S. M. Girvin, J. P. Carini, and D. Shahar, "Continuous quantum phase transitions," Rev. Mod. Phys. **69**, 315–333 (1997).

[11] Michael E. Fisher and Michael N. Barber, "Scaling theory for finite-size effects in the critical region," Phys. Rev. Lett. **28**, 1516–1519 (1972).

[12] E Brézin and Jean Zinn-Justin, "Finite size effects in phase transitions," Nuclear Physics B **257**, 867–893 (1985).

[13] Andreas Osterloh, Luigi Amico, Giuseppe Falci, and Rosario Fazio, "Scaling of entanglement close to a quantum phase transition," Nature **416**, 608–610 (2002).

[14] Zhangqi Zhu, Gaoyong Sun, Wen-Long You, and Da-Ning Shi, "Fidelity and criticality of a quantum ising chain with long-range interactions," Phys. Rev. A **98**, 023607 (2018).

[15] Myung-Joong Hwang and Martin B. Plenio, "Quantum phase transition in the finite jaynes-cummings lattice systems," Phys. Rev. Lett. **117**, 123602 (2016).

[16] R. Botet and R. Jullien, "Large-size critical behavior of infinitely coordinated systems," Phys. Rev. B **28**, 3955–3967 (1983).

[17] Harry J Lipkin, N Meshkov, and AJ Glick, "Validity of many-body approximation methods for a solvable model:(i). exact solutions and perturbation theory," Nuclear Physics **62**, 188–198 (1965).

[18] N Meshkov, AJ Glick, and HJ Lipkin, "Validity of many-body approximation methods for a solvable model:(ii). linearization procedures," Nuclear Physics **62**, 199–210 (1965).

[19] AJ Glick, HJ Lipkin, and N Meshkov, "Validity of many-body approximation methods for a solvable model:(iii). diagram summations," Nuclear Physics **62**, 211–224 (1965).

[20] Iris Cong, Soonwon Choi, and Mikhail D. Lukin, "Quantum convolutional neural networks," Nat. Phys. **15**, 1273–1278 (2019).

[21] Johannes Herrmann, Sergi Masot Llima, Ants Remm, Petr Zapletal, Nathan A. McMahon, Colin Scarato, François Swiadek, Christian Kraglund Andersen, Christoph Hellings, Sebastian Krinner, Nathan Lacroix, Stefania Lazar, Michael Kerschbaum, Dante Colao Zanuz, Graham J. Norris, Michael J. Hartmann, Andreas Wallraff, and Christopher Eichler, "Realizing quantum convolutional neural networks on a superconducting quantum processor to recognize quantum phases," Nat Commun **13** (2022), https://doi.org/10.1038/s41467-022-31679-5.

[22] Korbinian Kottmann, Friederike Metz, Joana Fraxanet, and Niccolò Baldelli, "Variational quantum anomaly detection: Unsupervised mapping of phase diagrams on a physical quantum computer," Phys. Rev. Research **3**, 043184 (2021).

[23] Joe Gibbs, Zoe Holmes, Matthias C. Caro, Nicholas Ezzell, Hsin-Yuan Huang, Lukasz Cincio, Andrew T. Sornborger, and Patrick J. Coles, "Dynamical simulation via quantum machine learning with provable generalization," (2022), 10.48550/ARXIV.2204.10269.

[24] Andrew Daley, Immanuel Bloch, Christian Kokail, Stuart Flannigan, Natalie Pearson, Matthias Troyer, and Peter Zoller, "Practical quantum advantage in quantum simulation," Nature **607**, 667–676 (2022).

[25] Sébastien Dusuel and Julien Vidal, "Continuous unitary transformations and finite-size scaling exponents in the Lipkin-Meshkov-Glick model," Phys. Rev. B **71**, 224420 (2005).

[26] J. I. Cirac, M. Lewenstein, K. Mølmer, and P. Zoller, "Quantum superposition states of Bose-Einstein condensates," Phys. Rev. A **57**, 1208–1218 (1998).

[27] D. A. Garanin, X. Martínez Hidalgo, and E. M. Chudnovsky, "Quantum-classical transition of the escape rate of a uniaxial spin system in an arbitrarily directed field," Phys. Rev. B **57**, 13639–13654 (1998).

[28] Octavio Castaños, Ramón López-Peña, Jorge G. Hirsch, and Enrique López-Moreno, "Classical and quantum phase transitions in the Lipkin-Meshkov-Glick model," Phys. Rev. B **74**, 104118 (2006).

[29] Jian Ma and Xiaoguang Wang, "Fisher information and spin squeezing in the Lipkin-Meshkov-Glick model," Phys. Rev. A **80**, 012318 (2009).

[30] Julien Vidal, Guillaume Palacios, and Claude Aslangul, "Entanglement dynamics in the Lipkin-Meshkov-Glick model," Phys. Rev. A **70**, 062304 (2004).

[31] Sébastien Dusuel and Julien Vidal, "Finite-size scaling exponents of the Lipkin-Meshkov-Glick model," Phys. Rev. Lett. **93**, 237204 (2004).

[32] Pedro Ribeiro, Julien Vidal, and Rémy Mosseri, "Exact spectrum of the Lipkin-Meshkov-Glick model in the thermodynamic limit and finite-size corrections," Phys. Rev. E **78**, 021106 (2008).

[33] Giulio Salvatori, Antonio Mandarino, and Matteo G. A. Paris, "Quantum metrology in Lipkin-Meshkov-Glick critical systems," Phys. Rev. A **90**, 022111 (2014).

[34] Antonio Mandarino, Karl Joulain, Melisa Domínguez Gómez, and Bruno Bellomo, "Thermal transistor effect in quantum systems," Phys. Rev. Applied **16**, 034026 (2021).

[35] D Agassi, HJ Lipkin, and N Meshkov, "Validity of many-body approximation methods for a solvable model:(iv). the deformed hartree-fock solution," Nuclear Physics **86**, 321–331 (1966).

[36] R. H. Dicke, "Coherence in spontaneous radiation processes," Phys. Rev. **93**, 99–110 (1954).

[37] Arnab Das, K. Sengupta, Diptiman Sen, and Bikas K. Chakrabarti, "Infinite-range ising ferromagnet in a time-dependent transverse magnetic field: Quench and ac dynamics near the quantum critical point," Phys. Rev. B **74**, 144423 (2006).

[38] S. Lerma H. and J. Dukelsky, "The Lipkin–Meshkov–Glick model as a particular limit of the su(1,1) Richardson–Gaudin integrable models," Nuclear Physics B **870**, 421–443 (2013).

[39] Gang Chen and JQ Liang, "Unconventional quantum phase transition in the finite-size Lipkin–Meshkov–Glick model," New Journal of Physics **8**, 297 (2006).

[40] Alberto Peruzzo, Jarrod McClean, Peter Shadbolt, Man-Hong Yung, Xiao-Qi Zhou, Peter J. Love, Alán Aspuru-

Guzik, and Jeremy L. O'Brien, "A variational eigenvalue solver on a photonic quantum processor," Nature Communications **5**, 4123 (2014).

[41] Jarrod R McClean, Jonathan Romero, Ryan Babbush, and Alán Aspuru-Guzik, "The theory of variational hybrid quantum-classical algorithms," New Journal of Physics **18**, 023023 (2016).

[42] Marcello Benedetti, Erika Lloyd, Stefan Sack, and Mattia Fiorentini, "Parameterized quantum circuits as machine learning models," Quantum Science and Technology **4**, 4 (2019).

[43] Jonathan Romero, Ryan Babbush, Jarrod R McClean, Cornelius Hempel, Peter J Love, and Alán Aspuru-Guzik, "Strategies for quantum computing molecular energies using the unitary coupled cluster ansatz," Quantum Sci. Technol. **4**, 014008 (2019).

[44] Abhinav Kandala, Antonio Mezzacapo, Kristan Temme, Maika Takita, Markus Brink, Jerry M. Chow, and Jay M. Gambetta, "Hardware-efficient variational quantum eigensolver for small molecules and quantum magnets," Nature **549**, 242–246 (2017).

[45] Luca Crippa, Francesco Tacchino, Mario Chizzini, Antonello Aita, Michele Grossi, Alessandro Chiesa, Paolo Santini, Ivano Tavernelli, and Stefano Carretta, "Simulating static and dynamic properties of magnetic molecules with prototype quantum computers," Magnetochemistry **7** (2021), 10.3390/magnetochemistry7080117.

[46] Panagiotis Kl. Barkoutsos, Jerome F. Gonthier, Igor Sokolov, Nikolaj Moll, Gian Salis, Andreas Fuhrer, Marc Ganzhorn, Daniel J. Egger, Matthias Troyer, Antonio Mezzacapo, Stefan Filipp, and Ivano Tavernelli, "Quantum algorithms for electronic structure calculations: Particle-hole hamiltonian and optimized wavefunction expansions," Phys. Rev. A **98**, 022322 (2018).

[47] E. F. Dumitrescu, A. J. McCaskey, G. Hagen, G. R. Jansen, T. D. Morris, T. Papenbrock, R. C. Pooser, D. J. Dean, and P. Lougovski, "Cloud quantum computing of an atomic nucleus," Phys. Rev. Lett. **120**, 210501 (2018).

[48] I. Stetcu, A. Baroni, and J. Carlson, "Variational approaches to constructing the many-body nuclear ground state for quantum computing," Phys. Rev. C **105**, 064308 (2022).

[49] Oriel Kiss, Michele Grossi, Pavel Lougovski, Federico Sanchez, Sofia Vallecorsa, and Thomas Papenbrock, "Quantum computing of the ^{6}li nucleus via ordered unitary coupled cluster," ArXiv e-prints (2022), arXiv:2205.00864 [nucl-th].

[50] Alexey Uvarov, Jacob D. Biamonte, and Dmitry Yudin, "Variational quantum eigensolver for frustrated quantum systems," Phys. Rev. B **102**, 075104 (2020).

[51] Maxime Dupont and Joel E. Moore, "Quantum criticality using a superconducting quantum processor," Phys. Rev. B **106**, L041109 (2022).

[52] Michael J. Cervia, A. B. Balantekin, S. N. Coppersmith, Calvin W. Johnson, Peter J. Love, C. Poole, K. Robbins, and M. Saffman, "Lipkin model on a quantum computer," Phys. Rev. C **104**, 024305 (2021).

[53] Kenneth Robbins and Peter J. Love, "Benchmarking near-term quantum devices with the variational quantum eigensolver and the Lipkin-Meshkov-Glick model," Phys. Rev. A **104**, 022412 (2021).

[54] Asahi Chikaoka and Haozhao Liang, "Quantum computing for the Lipkin model with unitary coupled cluster and structure learning ansatz," Chinese Physics C **46**, 024106 (2022).

[55] A. M. Romero, J. Engel, Ho Lun Tang, and Sophia E. Economou, "Solving nuclear structure problems with the adaptive variational quantum algorithm," Phys. Rev. C **105**, 064317 (2022).

[56] Manqoba Q. Hlatshwayo, Yinu Zhang, Herlik Wibowo, Ryan LaRose, Denis Lacroix, and Elena Litvinova, "Simulating excited states of the Lipkin model on a quantum computer," (2022), arXiv:2203.01478 [nucl-th].

[57] Harper R. Grimsley, Sophia E. Economou, Edwin Barnes, and Nicholas J. Mayhall, "An adaptive variational algorithm for exact molecular simulations on a quantum computer," Nat Commun **10**, 3007 (2019).

[58] Oscar Higgott, Daochen Wang, and Stephen Brierley, "Variational quantum computation of excited states," Quantum **3**, 156 (2019).

[59] Pauline J. Ollitrault, Abhinav Kandala, Chun-Fu Chen, Panagiotis Kl. Barkoutsos, Antonio Mezzacapo, Marco Pistoia, Sarah Sheldon, Stefan Woerner, Jay M. Gambetta, and Ivano Tavernelli, "Quantum equation of motion for computing molecular excitation energies on a noisy quantum processor," Phys. Rev. Research **2**, 043140 (2020).

[60] Jules Tilly, Glenn Jones, Hongxiang Chen, Leonard Wossnig, and Edward Grant, "Computation of molecular excited states on ibm quantum computers using a discriminative variational quantum eigensolver," Phys. Rev. A **102**, 062425 (2020).

[61] Ken M. Nakanishi, Kosuke Mitarai, and Keisuke Fujii, "Subspace-search variational quantum eigensolver for excited states," Phys. Rev. Research **1**, 033062 (2019).

[62] Paul D. Nation, Hwajung Kang, Neereja Sundaresan, and Jay M. Gambetta, "Scalable mitigation of measurement errors on quantum computers," PRX Quantum **2**, 040326 (2021).

[63] Andre He, Benjamin Nachman, Wibe A. de Jong, and Christian W. Bauer, "Zero-noise extrapolation for quantum-gate error mitigation with identity insertions," Phys. Rev. A **102**, 012426 (2020).

[64] Abhinav Kandala, Kristan Temme, Antonio D. Córcoles, Antonio Mezzacapo, Jerry M. Chow, and Jay M. Gambetta, "Error mitigation extends the computational reach of a noisy quantum processor," Nature **567**, 491–495 (2019).

[65] Lewis Fry Richardson, "The approximate arithmetical solution by finite differences of physical problems involving differential equations, with an application to the stresses in a masonry dam," Philosophical Transactions of the Royal Society of London, Series A, Containing Papers of a Mathematical or Physical Character **202**, 307–357 (1911).

[66] D. Kraft, *A Software Package for Sequential Quadratic Programming*, Deutsche Forschungs- und Versuchsanstalt für Luft- und Raumfahrt Köln: Forschungsbericht (Wiss. Berichtswesen d. DFVLR, 1988).

[67] Stuart M. Harwood, Dimitar Trenev, Spencer T. Stober, Panagiotis Barkoutsos, Tanvi P. Gujarati, Sarah Mostame, and Donny Greenberg, "Improving the variational quantum eigensolver using variational adiabatic quantum computing," ACM Transactions on Quantum Computing **3** (2022), 10.1145/3479197.

[68] Jerry M. Chow, A. D. Córcoles, Jay M. Gambetta, Chad Rigetti, B. R. Johnson, John A. Smolin, J. R. Rozen,

George A. Keefe, Mary B. Rothwell, Mark B. Ketchen, and M. Steffen, "Simple all-microwave entangling gate for fixed-frequency superconducting qubits," Phys. Rev. Lett. **107**, 080502 (2011).

[69] Gushu Li, Yufei Ding, and Yuan Xie, "Tackling the qubit mapping problem for nisq-era quantum devices," in *Proceedings of the Twenty-Fourth International Conference on Architectural Support for Programming Languages and Operating Systems*, ASPLOS '19 (Association for Computing Machinery, New York, NY, USA, 2019) p. 1001–1014.

[70] J.C. Spall, "Implementation of the simultaneous perturbation algorithm for stochastic optimization," IEEE Transactions on Aerospace and Electronic Systems **34**, 817–823 (1998).

[71] U. Schollwöck, "The density-matrix renormalization group," Rev. Mod. Phys. **77**, 259–315 (2005).

[72] Maria Schuld, Ville Bergholm, Christian Gogolin, Josh Izaac, and Nathan Killoran, "Evaluating analytic gradients on quantum hardware," Phys. Rev. A **99**, 032331 (2019).